# COMPARISON OF DIFFERENT APPROACHES FOR GUST MODELING IN THE CFD CODE TAU

Ralf Heinrich, Lars Reimer

DLR Institute of Aerodynamics and Flow Technology
Lilienthalplatz 7
38108 Braunschweig
ralf.heinrich@dlr.de, lars.reimer@dlr.de

**Keywords:** Gust response, Disturbance Velocity Approach, Resolved Gust Approach

**Abstract:** Two different methods for modeling of gusts have been implemented into the CFD-code TAU. The first one is the so called disturbance velocity approach, a simplified method which allows predicting the influence of a gust on the aircraft, but not the influence of the aircraft aerodynamics on the shape of the gust. Alternatively, an unsteady boundary condition has been implemented to feed in the gust into the flow field. Thereby the mutual interaction of gust and aircraft is captured. Both methods are compared in order to access the validity range of the simplified approach. A result is that for gust wavelength larger than two reference chords the agreement of the highly accurate method and simplified approach is good. For such cases the simplified approach has been used to simulate the gust interaction of a generic fighter aircraft and an A340 configuration, taking into account the reaction of the aircraft due to the additional loads.

## 1 INTRODUCTION

The prediction of unsteady loads caused by atmospheric effects like gusts is essential for aircraft development. The knowledge of the additional loads arising is of importance for the design of the structure but also for the layout of the control surfaces and the Flight-Control-System (FCS). To predict these additional air-loads two different approaches for gust-modeling have been implemented in the CFD-code TAU [1].

One of these methods for modeling of gusts is the so called Disturbance Velocity Approach (DVA), see for example [2]. This method is straight forward to implement in CFD-codes and allows the usage of standard meshes, which usually are characterized by a reduced mesh resolution with growing distance from the aircraft. The method captures the influence of the gust on the aircraft, but is not able to predict the feedback of the aerodynamics of the aircraft on the gust shape. Therefore, especially for gusts of short wavelength, a prediction error can be expected. To get a clearer view of the range of validity of the DVA an alternative method has been implemented in TAU: The gust can be fed into the discretized flow field using an unsteady boundary condition at the far-field boundaries. The advantage of the method is that the mutual interaction of gust and aircraft is captured, since the gust is resolved in the flow field. Therefore the abbreviation of this approach is RGA in the following standing for Resolved Gust Approach. However, a high resolution in the whole domain is required, to transport a gust from the inflow boundary to the aircraft without too much numerical losses.

In the following the DVA is described at first and, afterwards, the strategy to simulate the mutual interaction using the unsteady boundary condition. A comparison of both approaches is

presented in chapter 2.3. To demonstrate the capability of the DVA for industrial applications, the interaction of a generic fighter aircraft with a lateral gust is presented in chapter 3. Here, this simulation the reaction of the aircraft due to the additional loads is captured by coupling of aerodynamics and flight-mechanics.

## 2 GUST MODELING IN TAU

### 2.1 Disturbance Velocity Approach

To enable the simulation of an aircraft interacting with atmospheric effects, several approaches are possible. One popular method is the DVA, which has been implemented into the block structured DLR FLOWer code [3] for the simulation of the influence of wake-vortices of a large leading aircraft model on the loads of a smaller aircraft model following [2]. Good agreement to experimental data was found. Motivated by the success of this method, the DVA has now also been implemented into the hybrid TAU-code.

In this method the flux balance is slightly altered by superposition of an additional disturbance velocity field $\mathbf{v}_i$ induced by e.g. a gust. $\mathbf{v}_i$ is prescribed as a function of space and time, depending on the shape and position of the gust. The convection across the cell interface of a control volume changes from $\mathbf{v} - \mathbf{v}_b$ to $\mathbf{v} - \mathbf{v}_b - \mathbf{v}_i$. with $\mathbf{v}_b$ being the velocity of the boundary of a control volume. For example the continuity equation then changes to

$$\frac{d}{dt}\int_V \rho dV + \oint_S \rho(\mathbf{v} - \mathbf{v}_b - \mathbf{v}_i)dV = 0 \quad . \tag{1}$$

**Fig. 1** shows a gust with wavelength $\lambda_{gust}$ moving with a speed of $u_{inf}$ relative to an airfoil. The shape of the gust is specified as a function of the coordinate $x$ and time $t$. In **Fig. 1** left ($t = 0$), the gust is in front of the airfoil. The velocity $\mathbf{v}_i$ induced by the gust at the interface of the control volume is **0**. In the right part of **Fig. 1** the gust is just beneath the airfoil ($t = t_1$). The induced velocity is now equal to the amplitude of the gust. The local effect of the gust is approximately the same, as if the airfoil is moving with the negative gust vertical speed $\mathbf{v}_{gust}(x,t)$ downward. More about the motivation and verification of this method may be found in [4].

In TAU, gusts with a "1-cos" shape as described in the Federal Aviation Regulations (FAR) part 25.341 can be defined or, alternatively, sharp edge gusts, see **Fig. 2** left. The amplitude of the gust $w_{gust}$ and the wavelength $\lambda_{gust}$ are input parameters. Vertical as well as lateral gusts can be specified. The user can select between isolated gusts and sequences of gusts. The extension of the gusts in spanwise direction (vertical gusts) and vertical direction (lateral gusts) can also be specified. **Fig. 2** right shows as example a generic fighter aircraft encountering a sequence of three vertical gusts restricted in spanwise direction and a single lateral gust.

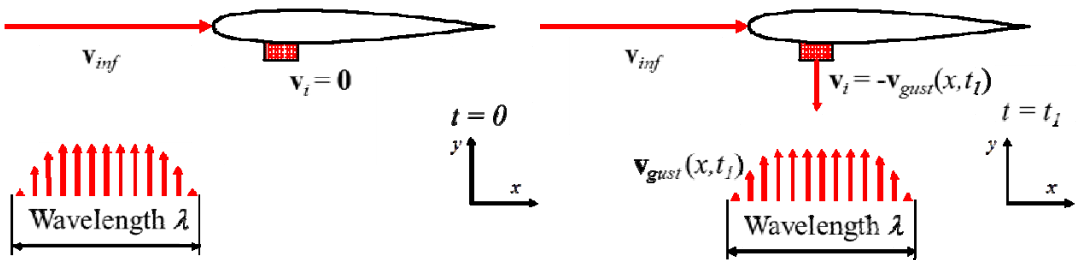


**Fig. 1.** Gust traveling relative to an airfoil

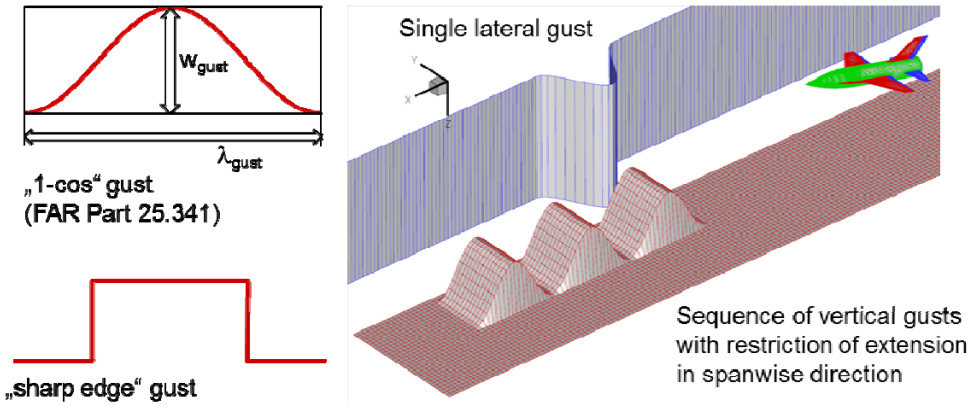


**Fig. 2.** Left: Gust shapes allowed in TAU. Right: Aircraft encountering a sequence of three vertical gusts (with restriction of the extension in spanwise direction) and a single lateral gust

## 2.2 Resolved Gust Approach

To enable the simulation of a mutual interaction of aircraft and gust, the resolution of the gust in the flow field is required. This can be realized by feeding the gust into the flow field at the far field boundary. Therefore, in TAU, the non-reflecting far field boundary condition based on the work of Whitfield [5] has to be adapted. For this boundary condition a far field state including velocity components $u_{inf}$, $v_{inf}$, $w_{inf}$ has to be specified at the outer side of the discretized domain. Usually these values are constant at the whole far field boundary. For gust simulations the velocity components of the far field state can now be specified as a function of space and time.

As already mentioned a disadvantage of the approach is the requirement of high spatial resolution to transport the gust without too much numerical losses, since TAU is only of 2nd order accuracy in space. To minimize the effort necessary to transport a gust through the discretized flow domain from inflow boundary to the aircraft, a technique making use of “gust-transport-meshes” has been developed. The idea behind will be described for a 2D test case, which has been set up to compare the DVA and the RGA approach: The interaction of a symmetrical NACA0012 airfoil with a Horizontal Tail Plane (HTP) with a vertical gust. The reason for selection of this configuration is the expectation, that the aerodynamic of the wing will have an influence on the shape of the gust, which afterwards interacts with the HTP. This effect is not captured with the DVA, but with the RGA. So, if the effect is of relevance, this test case will give an answer on the magnitude of the prediction error regarding e.g. maximum loads acting on the configuration.

The grid used in this example is an overset mesh, as shown in **Fig. 3**. An unstructured mesh containing wing and HTP (blue) are placed into a Cartesian background mesh (red). The distance between inflow boundary and wing is 20 chord lengths. A higher resolution normal to the wing plane is used close to the airfoils (up to a distance of z = ±3 chord lengths). The spacing is increased with growing distance from the airfoils, in order to safe mesh nodes. An additional grid (green) with a high resolution in flow direction is used for the “transport” of the gust from the far field boundary to the wing-HTP configuration. For time $t = 0s$, the gust is just in front of the computational domain. For time $t > 0s$, the gust is fed into the flow field at the left and the lower far field boundary marked blue in **Fig. 3**. The position of the gust transport grid is unchanged, until the gust is centered in the gust transport mesh. Afterwards the grid is starting to move with the convection velocity $u_{inf}$ of the flow.

To find an appropriate resolution of the gust transport mesh, a grid density study has been made, using only the background grid and the gust transport grid. We assume a short gust wavelength of only one grid unit, corresponding to the reference chord length of the wing (cases with longer wavelength are less critical). As gust amplitude 10% of the convection speed is selected. Three different resolutions in flow direction have been tested: 25, 50 and 100 cells to resolve one gust wavelength.

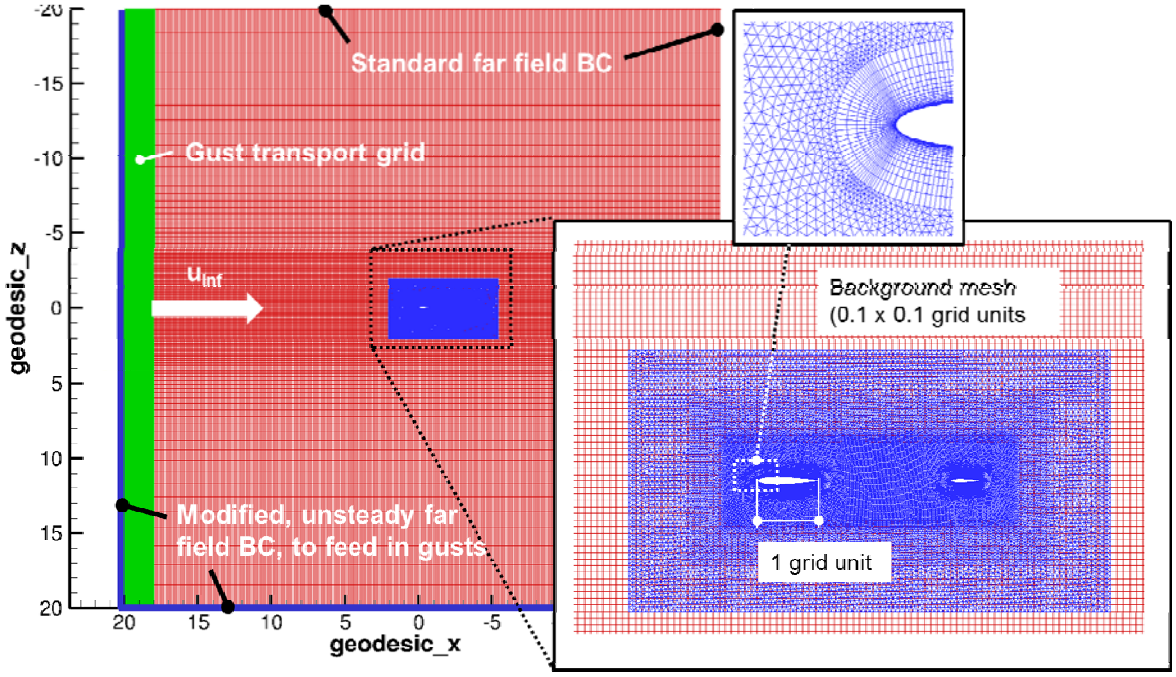


**Fig. 3.** Overset grid setup for simulation of interaction of wing-HTP configuration with a gust of wavelength 1 grid unit (plotted in inertial (geodesic) coordinate system)

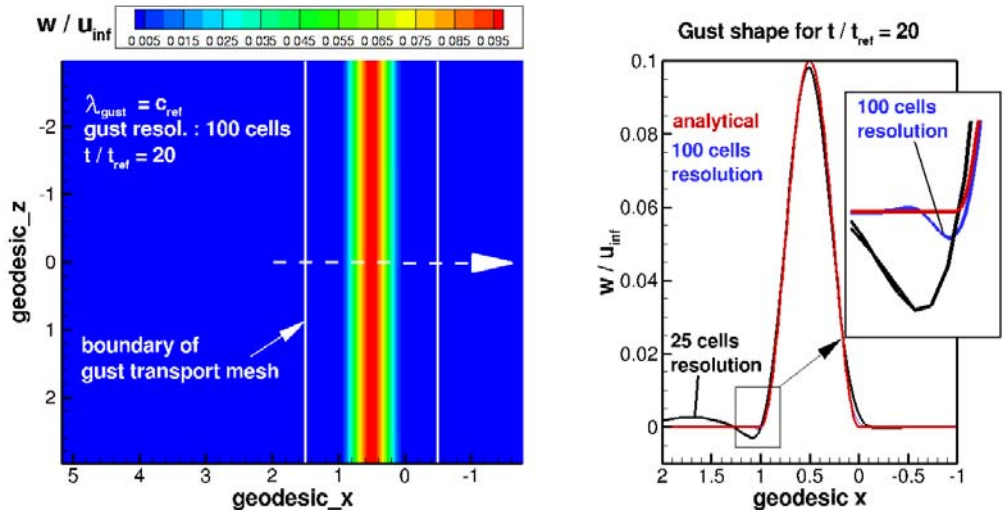


**Fig. 4.** Left: Zoom-in of computed *z*-velocity distribution normalized with $u_{inf}$ after gust has travelled 20 grid units. 100 cells have been used for one gust wavelength). Right: Corresponding velocity profile for $z = 0$ for a resolution of 25 and 100 cells for one gust wavelength, compared to analytical solution (unchanged "1-cos" shape)

**Fig. 4** left shows the z-velocity (*w*) distribution of a zoom-in of the flow field, after the gust has travelled already 20 chord lengths using a resolution of 100 cells for one gust wavelength.

This is the travelling distance of the gust between far field and wing needed later on for comparison of DVA and RGA approaches in chapter 2.3. The contour lines are still straight lines, as could be expected for an appropriate resolution of the gust. A more detailed view of the resulting velocity profile for $z = 0$ is presented in **Fig. 4** right (same $z$-position as of the wing-HTP configuration used in the simulations for comparison of DVA and RGA approach described below). The solid red line is the analytical solution (gust shape unchanged after 20 chord lengths travelled distance). The black line shows the result using 25 cells for gust resolution. Compared to the analytical solution the amplitude of the gust is slightly reduced. Deviations from the analytical solution are especially visible left of the gust. The blue line corresponds to the result using a resolution of 100 cells. The comparison to the analytical solution is very good (the blue line is covered almost entirely by the red line). Only minor deviations are visible at the base of the gust, see zoom-in in **Fig. 4**, right. For the comparison of both approaches a resolution of 100 cells is used to be on the safe side.

## 2.3 Comparison of Both Approaches

Computations have been made for 3 different gust wavelengths (1, 2 and 4 wing chord-lengths). As in the study in the previous chapter the classical "1-cos" gust shape has been selected. Two different on-flow Mach numbers are used, to allow checking the influence of compressibility. For the Mach number of $Ma_{inf} = 0.25$, we expect nearly incompressible flow, whereas compressibility effects can be expected for $Ma_{inf} = 0.75$. The gust amplitude is 10% of the on-flow velocity. The angle of attack $\alpha$ is 0°. Since the airfoils of wing and HTP are symmetrical, the resulting lift is purely created by gust loading. Inviscid as well as viscous computations have been made. For the viscous simulations a higher grid density in wall normal direction of the airfoil meshes is selected, to resolve the boundary layer properly. The original version of the Spalart-Allmaras turbulence model has been used. The Reynolds number is $5.83 \times 10^6$ for $Ma_{inf} = 0.25$ and 17.5 $Ma_{inf} = 0.75$.

As measure for the prediction error of the DVA relative to the RGA approach, the maximum lift found during the simulation is used:

$$err_{C_{L,\max}} = \frac{\left|C_{L,\max,RG} - C_{L,\max,DVA}\right|}{\left|C_{L,\max,RG}\right|} \tag{2}$$

The resulting errors for both Mach numbers and the 3 wavelengths are discussed below and summarized in **Table 1**. **Fig. 5** shows the comparison of results of the DVA (dashed lines) and the more accurate RGA approach (solid line). The lift history computed for all three wavelengths is plotted versus dimensionless time. Time has been made dimensionless using the time $t_{ref}$ of a gust needed to travel a distance of one reference chord length $c_{ref}$ with velocity $u_{inf}$ ($t_{ref} = c_{ref} / u_{inf}$). The agreement of the simple approach with the accurate approach predicting the mutual interaction is surprisingly well! Nearly no difference is visible for the wavelength of 4 and 2 chord length for $Ma = 0.25$. The error of the DVA for prediction of the maximum lift is only *0.21%* for $\underline{\lambda} = \lambda / c_{ref} = 4$ and *1.16%* for $\underline{\lambda} = 2$. The situation is similar for $Ma_{inf} = 0.75$, but compared to nearly incompressible flow the prediction error is higher (*2.72%* for maximum lift for $\underline{\lambda} = 2$). But all in all the discrepancy between DVA and RGA approach is acceptable.

A clearer difference is visible for the short wavelength of 1 chord length for dimensionless time between 23 and 25 for both Mach numbers, corresponding to the time when gust and HTP interact. The peaks are over-predicted by the DVA, since this method does not capture

the effect of the wing aerodynamic on the gust shape. Additionally the maximum lift found with the DVA is under-predicted for $Ma_{inf}$ = 0.75, see also zoom-in in **Fig. 5** right. The error of 10.69% is not acceptable. For the incompressible regime the error in is still below 2%, which is acceptable.

**Fig. 6** shows the same comparison as in **Fig. 5** for viscous computation. The general trend is very similar compared to inviscid simulations. The largest error again occurs for the shortest wavelength and the smallest error for the largest wave length, as expected.

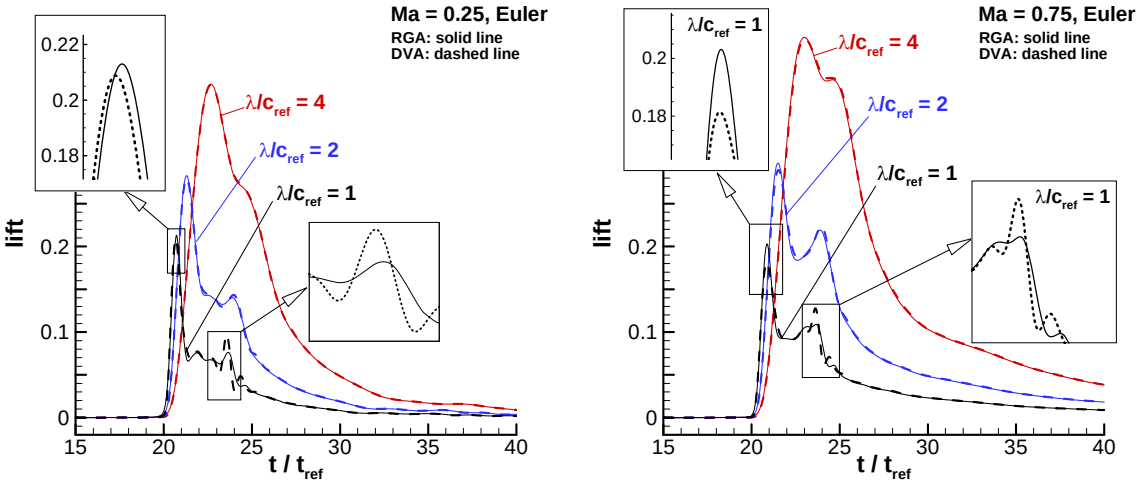


**Fig. 5.** Comparison of lift versus dimensionless time predicted by DVA and RGA approach (inviscid)

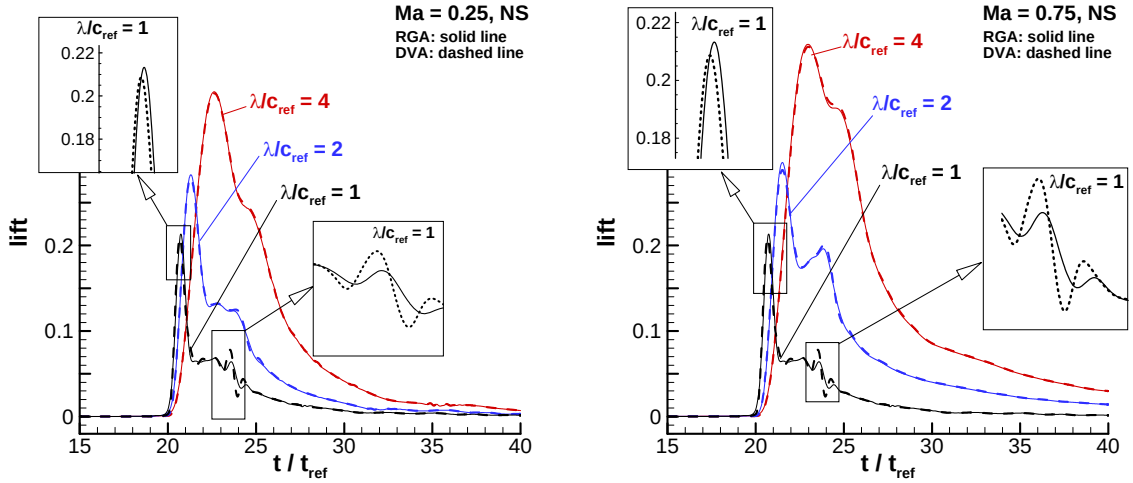


**Fig. 6.** Comparison of lift versus dimensionless time predicted by DVA and RGA approach (viscous)

| λ / cref | $err_{CL,max}$ [%] | | | |
|---|---|---|---|---|
| | Ma = 0,25 | | Ma = 0,75 | |
| | Euler | NS | Euler | NS |
| 1 | 1,96 | 2,16 | 10,69 | 11,08 |
| 2 | 1,16 | 1,24 | 2,72 | 2,93 |
| 4 | 0,21 | 0,47 | 0,42 | 0,64 |

**Table 1.** Maximum lift prediction error of DVA and RGA approach

## 3 APPLICATIONS

### 3.1 Simulation of Generic Fighter Aircraft Encountering a Lateral Gust

To demonstrate the simulation of a gust encounter, as geometry the so-called SDM configuration [6] has been selected, which is a generic fighter configuration similar to an F16. We assume the aircraft is set to fly horizontally at sea level with a Mach number of $Ma_{inf}=0.5$. We assume that the aircraft encounters a gust ("1-cos" shape) with a wavelength $\lambda_{gust}$ of *30m*, which corresponds to a non-dimensional wavelength $\underline{\lambda}$ of nearly *10*. In that case the DVA is a good choice for modeling the gust. The gust amplitude is $w_{gust} = 30m/s$. To take into account the reaction of the aircraft, TAU is coupled to a six degree of freedom flight-mechanics module. For details of the coupling procedure and the flight-mechanics module, the reader is referred to [4].

**Fig. 7** left shows the situation when the gust is just beside the aircraft. The grey sinusoidally shaped geometry represents the position and shape of the gust relative to the aircraft. The effect of the gust is an increase of side slip angle. Therefore a lateral force $F_y$ is created pushing the aircraft in negative $y_g$ direction (subscript "*g*" stands for the geodesic inertial coordinate system). This is also a result of the simulation as can be seen in the plot of the time history in **Fig. 7** right. One portion of the lateral force ($F_{y,VTP}$) is acting on the vertical tail plane, creating a rolling and a yawing moment $M_x$ and $M_z$. Therefore we expect a damped yawing and rolling motion. As the gust is coming from starboard position, we do not expect a large influence on the angle of attack, the pitching moment and the pitching angle Θ. The expectations are confirmed by the computed time history of the Euler angles plotted in **Fig. 7**.

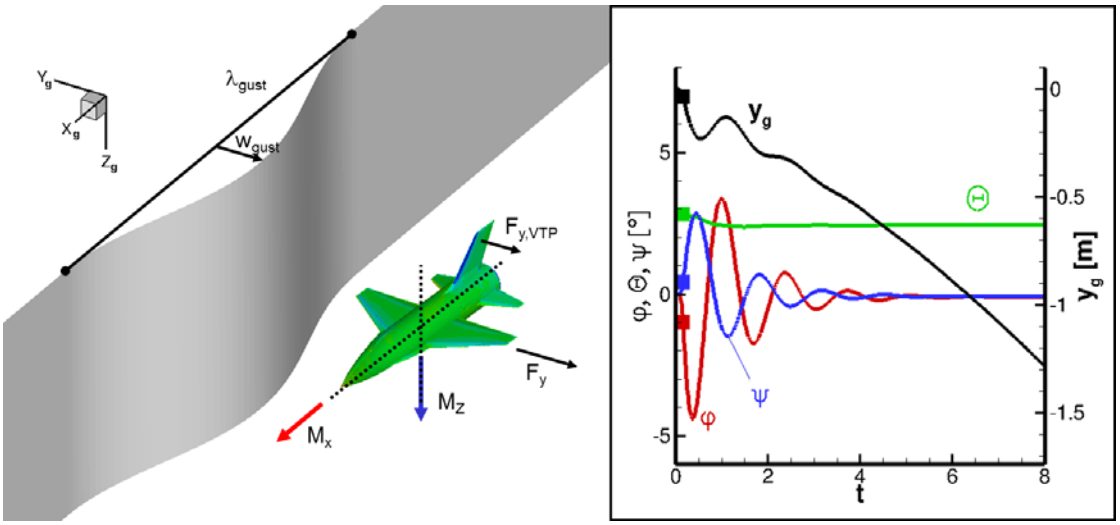


**Fig. 7.** Lateral gust encounter of generic fighter aircraft. Right: History of Euler angles & lateral position of center of gravity

### 3.2 Simulation of encounter of an A340 cruise configuration with a vertical gust

To demonstrate the capability of the process chain for an industrial application, the interaction of an Airbus A340-300 configuration with a generic sinusoidal gust is presented. This is the same configuration which has been used in the project AWIATOR (Aircraft Wing with Advanced Technology Operation) funded by the European Union. We assume that the aircraft has a weight of 195 tons and is flying at a height of 12.6 km with a dimensionless speed of

$Ma_\infty$ = 0.85. This corresponds to a Reynolds-number of $35.3 \times 10^6$. For current application we use a vertical gust with a wave-length $\lambda$ of 60m and an amplitude $U_{ds}$ of 15m/s. The wave-front is perpendicular to the horizontal flight path. Since the configuration is symmetric, only two translational degrees of freedom (in flight direction and normal to the wing plane) and a single rotational degree of freedom (pitch) are active. The Spalart-Allmaras model (original version) has been used as turbulence model.

A hybrid mesh for the full configuration with about 12 million nodes for the jig shape of the aircraft has been generated with the CENTAUR software [7]. In contrary to previous test cases also elastic effects are taken into account by coupling to NASTRAN [8] using the procedure described e.g. in [9]. Before the unsteady coupled computation is started, the initial conditions for horizontal flight are computed using the trim algorithm described in [10]. Therefore for each trim iteration the aeroelastic equilibrium has been computed. **Fig. 8** shows in grey the initial configuration (jig-shape) as well as the configuration in aeroelastic equilibrium. On the surface of the equilibrium configuration the pressure coefficient distribution is plotted. The diagram top of **Fig. 8** shows the convergence history of the trim process. Input parameters of the trim computation are the angle of the HTP $\eta_{HTP}$ (solid red line), the thrust and the pitch angle. Since the aircraft is flying in the linear range of lift and pitching moment coefficient the Newton iteration converged in only 2 steps. The resulting force in vertical direction balances the weight of the aircraft ($F_{z,g}$ – weight = 0, solid blue line), the resulting pitching moment coefficient including contribution from the thrust vanishes (dashed blue line) and the resulting force in x direction equals zero.

The trimmed state has been verified by starting an unsteady coupled computation (CFD, 6-DOF-module and structure model[1]) without gust disturbance. As expected, the height above ground as well as the pitch angle remains constant during one minute of real flight simulation. Thereafter, the gust encounter simulation has been started using a timestep size of 0.01s.

**Fig. 9** to **Fig. 11** show the situation for three different snapshots of the unsteady simulation as well as of the history of the pitching moment coefficient ($C_{my}$), the load factor (weight – resulting force in z-direction normalized with the weight) and the pitching angle $\Theta$. The respective times of the snapshots are marked with filled circles on top of the curves. Two different simulations have been carried out. In the first simulation (solid red curves) TAU has been coupled to flight mechanics and structure mechanics and the second simulation has been mono-disciplinary using the CFD mesh in flight shape stemming from a previous calculation of the trimmed state (dashed blue curves).

**Fig. 9** represents the initial situation when the gust is still far away (in front of the aircraft), having no influence on the aircraft. The grey sinusoidal shaped plane illustrates the position of the gust relative to the aircraft. The flow around the aircraft is still undisturbed and the aircraft is still in equilibrium. The aircraft is flying horizontally with constant speed, the load factor is 0, the pitching moment coefficient is 0 and thus the pitch angle remains constant. Afterwards, the aircraft starts to interact with the gust. The effect of a vertical gust is the same as increasing the AoA. This results in an enlargement of the lift and the vertical acceleration. The wings are bending upwards relative to the flight shape (in grey). The maximum effect is

[1] For this first CFD – flight mechanics – structure coupling simulation, on structure side only the steady problem has been solved for each physical time step with the actual aerodynamic loads and thrust (quasi steady mode). Structure coupling using a modal approach is ongoing work.

achieved, when the center of the gust (maximum vertical speed) is close to the aerodynamic center of the wing. This situation corresponds to **Fig. 10**. The load factor is about -0.5 and the aircraft starts to move upward. The sign of the load factor / acceleration is negative, because it is expressed in geodesic coordinates ($z_g$ pointing downward). In that stage already an influence of the upwind of the gust on the HTP is visible. The increased local AoA results in a vertical force acting on the HTP, which contributes to a "nose down" pitching moment. Consequently the pitch starts to be reduced. Even after the gust has passed, the pitch angle is still decreasing, due to the effect of the aircraft's inertia. After the gust has passed, the AoA is reduced, which is comparable to undisturbed flight. Consequently, the load factor expressed in geodesic coordinates is now positive (pointing downward). This corresponds to $t \sim 0.7s$. The second effect is that now a "nose up" pitching moment is acting. The pitch angle is increased again. After ~1.4*s*, the initial pitch angle is reached again. Due to the effect of inertia, the pitch is further increased, resulting again in a "nose down" pitching moment. The behavior of the pitch angle is similar to a damped oscillation, which is expected from a stable flying aircraft. **Fig. 11** shows the situation after 2s (the gust is already far away), the maximal pitch angle has been reached and the aircraft has moved upward. In summary, the multidisciplinary simulation results are in agreement with what is expected from an aircraft interacting with a sinusoidal gust.

In the mono-disciplinary simulations the pitch angle is constant (only 0.6 s have been simulated). It can be seen that the load factor is over-predicted compared to the multi-disciplinary simulations because the reaction of the aircraft has not been taken into account. This could result in a heavier aircraft with reduced performance properties.

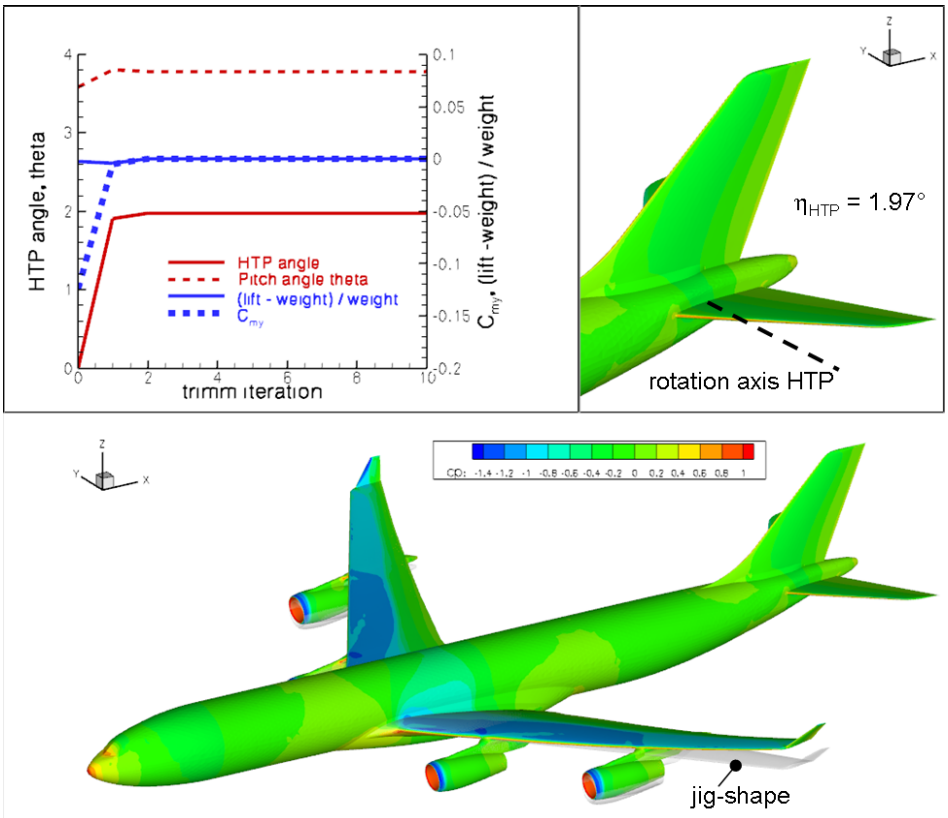


**Fig. 8.** A340-300 configuration in aeroelastic equilibrium as well as the history of the trim procedure

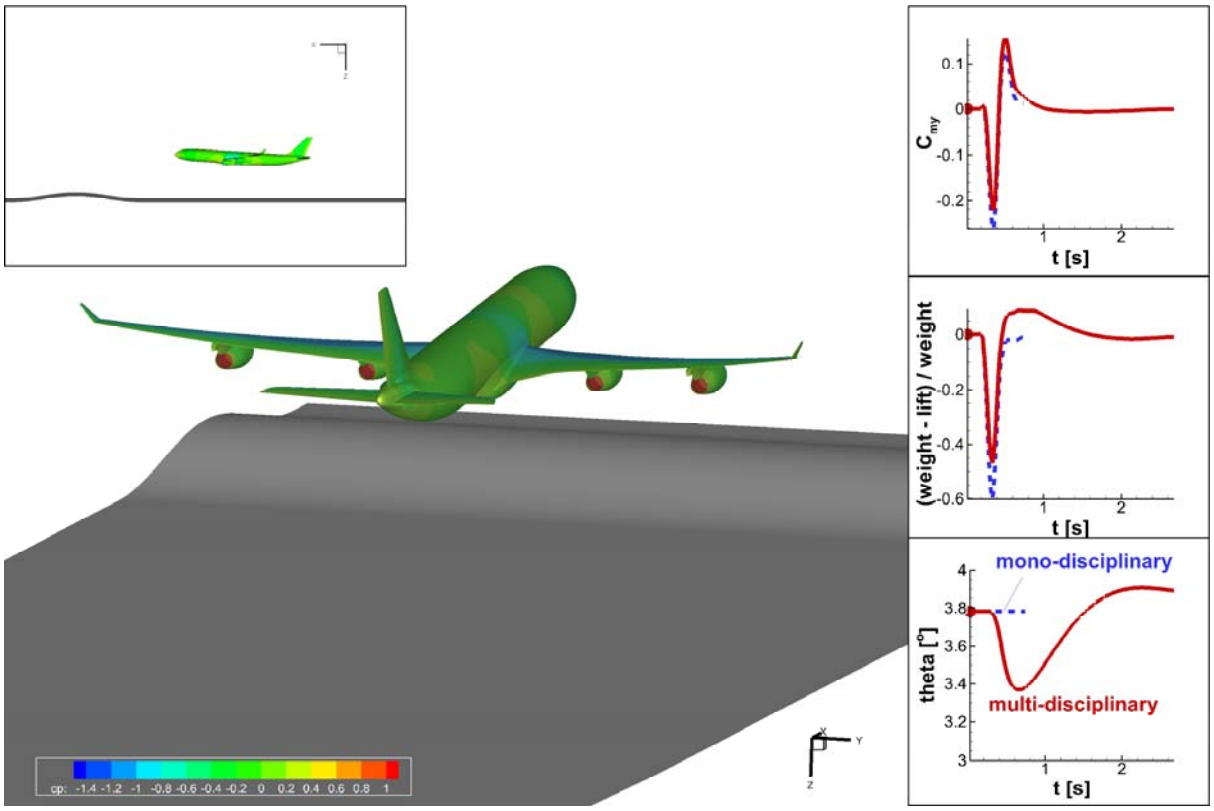


**Fig. 9.** Interaction of A340-300 configuration with a vertical gust for t = 0s (gust in front of the aircraft)

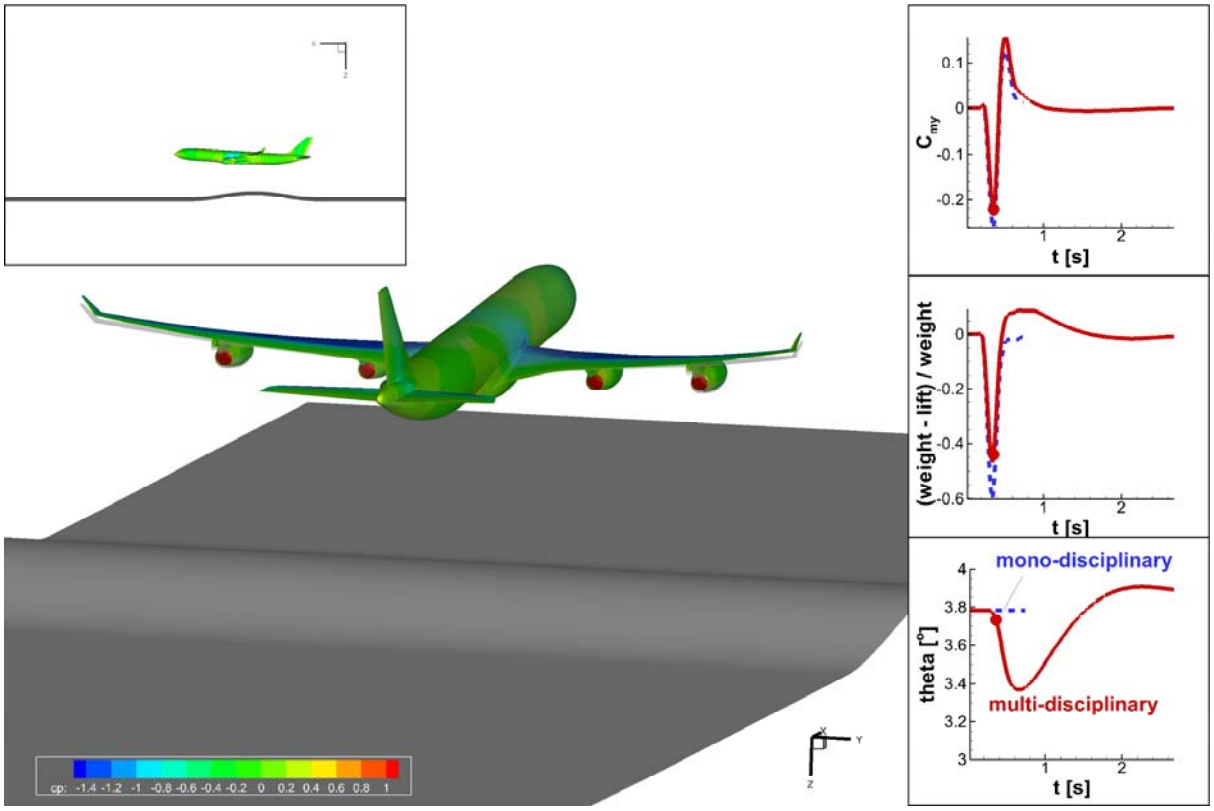


**Fig. 10.** Interaction of A340-300 configuration with a vertical gust (gust beneath the aircraft)

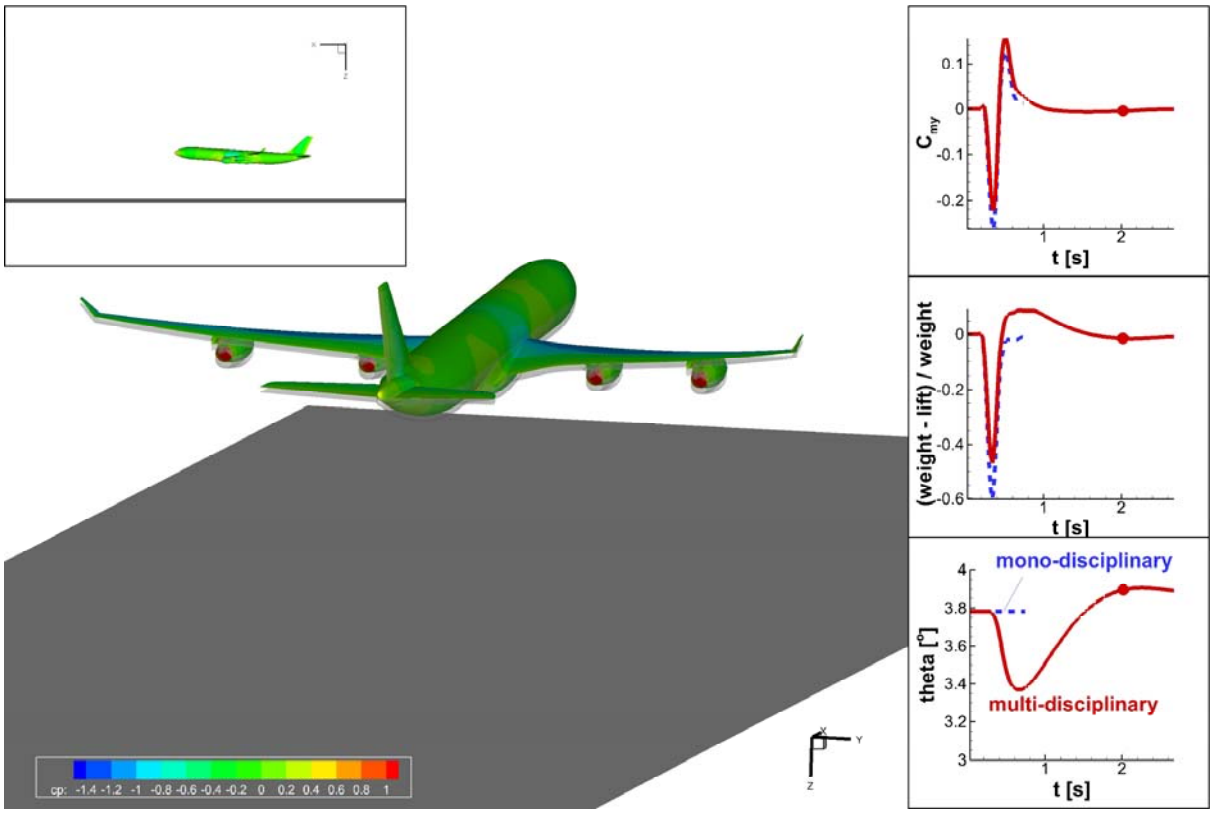


**Fig. 11.** Interaction of A340-300 configuration with a vertical gust (gust has passed the aircraft)

## 4 SUMMARY AND CONCLUSIONS

Two different methods for modeling of gusts have been implemented into the CFD-code TAU:

1. A simplified method called disturbance velocity approach allowing the usage of standard CFD meshes. The disadvantage is that the mutual interaction of gust and aircraft is not captured;
2. A method resolving gusts in the flow field, allowing the simulation of a mutual interaction of aircraft and gusts. They are fed into the flow field via an unsteady boundary condition. The disadvantage is that a high mesh resolution is required to resolve the gusts properly.

A comparison for a 2D wing-HTP configuration shows that the prediction quality of the simplified approach is comparable to the highly accurate method for dimensionless gust wavelengths $\underline{\lambda} = \lambda / c_{ref}$ down to a value of 2. For shorter wavelengths, especially for compressible flow, the prediction error is not negligible. The applicability of the disturbance velocity approach for industrial configuration has been demonstrated for the simulation of the interaction gust with a generic fighter aircraft and a commercial transport aircraft. For the future it is planned to undertake a comparison of both approaches for 3D configurations with fuselage.

## 5 REFERENCES

[1] Schwamborn, D., Gerhold, T., Heinrich, R.: The DLR TAU-Code: Recent Applications in Research and Industry. In Proceedings of "European Conference on Computational Fluid Dynamics" ECCOMAS CDF 2006, Egmond aan Zee, The Netherland, 2006

[2] Heinrich, R.: Numerical Simulation of Wake-Vortex Encounters Using the Chimera-Technique. STAB-Symposium 2000 in Stuttgart, in New Results in Numerical and Experimental Fluid Mechanics III, Springer, 2002

[3] Kroll, N., Fassbender, J. K. (eds): MEGAFLOW - Numerical Flow Simulation for Aircraft Design. Notes on Numerical Fluid Mechanics and Multidisciplinary Design (NNFM), 89, Springer-Verlag, 2005

[4] Ralf Heinrich, Andreas Michler: Unsteady Simulation of the Encounter of a Transport Aircraft with a Generic Gust by CFD Flight Mechanics Coupling, CEAS Conference 2009, Manchester, 2009

[5] Whitfield, D. L., Three-dimensional unsteady Euler Equation solutions using flux vector splitting, NASA contractor report NASA CR-173254, 1983

[6] S. Zan et al: Wing and Fin Buffet on the Standard Dynamic Model, RTO Technical Report, RTO-TR-26, pp 361-381, 2000

[7] http://www.centaursoft.com

[8] http://www.mscsoftware.com

[9] R. Heinrich, N. Kroll, J. Neumann, B. Nagel: Fluid-Structure Coupling for Aerodynamic Analysis and Design – A DLR Perspective, 46th AIAA Aerospace Sciences Meeting and Exhibit 2008, Reno, paper 2008-056, 2008

[10] Michler, A., Heinrich, R.: Numerical Simulation of the Elastic and Trimmed Aircraft. In Notes on Numerical Fluid Mechanics and Multidisciplinary Design (NNFM), Vol. 112: New Results in Numerical and Experimental Fluid Mechanics VII, Dillmann, A., Heller, G., Klaas, M., Kreplin, H.-P., Nitsche, W., Schröder, W. (eds). Springer-Verlag, 2010